Applied Catalysis B: Environmental 101 (2011) 560–569

Contents lists available at ScienceDirect

Applied Catalysis B: Environmental

journal homepage: www.elsevier.com/locate/apcatb

Gold nanoparticles supported on hydroxylapatite as high performance catalysts for low temperature CO oxidation

Jun Huang[a], Lu-Cun Wang[b], Yong-Mei Liu[a], Yong Cao[a,*], He-Yong He[a], Kang-Nian Fan[a]

[a] Shanghai Key Laboratory of Molecular Catalysis and Innovative Materials, Department of Chemistry, Fudan University, Shanghai 200433, PR China
[b] Institute of Surface Chemistry and Catalysis, Ulm University, D-89069 Ulm, Germany

ARTICLE INFO

Article history:
Received 28 July 2010
Received in revised form 7 October 2010
Accepted 23 October 2010
Available online 30 October 2010

Keywords:
Hydroxyapatite
Supported gold catalysts
Calcination atmosphere
CO oxidation
Catalyst stability

ABSTRACT

A series of gold supported on hydroxylapatite (HAP) catalysts were prepared by deposition–precipitation with urea to study the influence of calcination atmosphere, i.e., H_2, He and O_2, on the performance of the catalyst in low-temperature CO oxidation. Calcination atmosphere was found to have an important influence on the catalytic activity and stability of Au/HAP. The highest initial activity was obtained for Au/HAP-He obtained by inert He-calcination, which, however, suffered the most severe deactivation with time on stream. Calcination in oxidative O_2 environment resulted in the best stability and highest steady-state activity among the three catalysts. TEM results revealed that inert He-calcination can produce the smallest Au nanoparticles over the HAP support, which was suggested to be responsible for the highest initial activity of Au/HAP-He. Based on the CO_2-TPD and in situ DRIFTS studies, the superior stability of Au/HAP-O_2 can be attributed to a limited surface basicity in this material.

1. Introduction

Carbon monoxide is one of the main toxic gaseous pollutants which is generally produced and released from the combustion process of fossil fuels [1–3]. Catalytic oxidation of carbon monoxide to carbon dioxide at low temperature has been of considerable interest due to its significance in many industrial applications as well as to meet stringent environmental regulations [4–6]. In recent years, supported gold catalysts have attracted tremendous attention owing to the pioneering discovery by Haruta that catalysts containing nanosized gold particles (<5 nm) have extraordinary activities for low temperature CO oxidation [2]. Compared to traditional metal oxide catalysts such as NiO, Co_3O_4 and Hopcalite [7] and Pt- or Pd-based metal catalysts [8], Au catalysts can be an order of magnitude more active [9,10]. In particular, suitably prepared gold catalysts can oxidize CO at a temperature as low as −70 °C [2,11].

One of the most important limitations in the use of gold catalysts is their progressive deactivation during the catalytic test [12,13]. In this context, the poor long-term stability during the CO oxidation is a key deficiency that could hamper the practical applications of gold-based catalysts. It is well established that catalytic activity and stability of supported gold depend strongly on the preparation method [11,14,15], the gold particle size [9,16], pretreatment conditions [17–19], the reaction atmosphere [20,21], in particular the choice of the supports [22,23] and the specific interaction between gold and the support [24]. Therefore, considerable recent interest in gold catalysis has been directed toward finding a more suitable support for stabilizing Au nanoparticles. Among all supporting materials investigated, non-oxides, in particular various metal phosphates including $FePO_4$ [25], $LaPO_4$ [26] and $BaCO_3$ [27] are identified as promising supports for anchoring gold, some of them display excellent stability in low temperature CO oxidation.

Hydroxyapatite ($Ca_{10}(PO_4)_6(OH)_2$, denoted as HAP), a phosphate mineral having flexible structure, superior ion-exchange capacity, extraordinarily chemical and thermal stability and tunable surface acidic/basic properties, is of considerable interest owing to its potential usefulness as biomaterials, adsorbents and ion-exchangers [28]. The possession of both amphoteric and ion-exchange functions makes HAP appealing as more suitable carrier for a number of catalytic applications [29–31]. However, HAP has received limited attention as supports for gold nanoparticles [30,31], especially in the field of CO oxidation. Recently, Phonthammachai et al. reported that gold loaded on ceramic HAP foams are highly stable for CO oxidation [32], although a reasonable reaction rate requires a temperature higher than 100 °C. More recently, Domínguez et al. demonstrated that gold deposited on carbonated HAP can show prominent activity for CO oxidation at room temperature [33], but the stability of the catalyst remained unknown.

The present work is devoted to the understanding of the essential features of the catalysis of the gold nanoparticles loaded HAP (Au/HAP) in low temperature CO oxidation. Gold introduced to the

* Corresponding author. Tel.: +86 21 55665287; fax: +86 21 65643774.
E-mail address: yongcao@fudan.edu.cn (Y. Cao).

0926-3373/$ – see front matter © 2010 Elsevier B.V. All rights reserved.
doi:10.1016/j.apcatb.2010.10.029

Table 1
Physicochemical properties, catalytic activities and activation energies for various Au/HAP catalysts calcined under different atmospheres.

Catalysts	S_{BET} ($m^2\,g^{-1}$)	V_p ($cm^3\,g^{-1}$)	d_p (nm)	d_{Au}[a](nm)	T_{50}[b](°C)	r_{Au}[c]($mmol_{CO}\,g_{Au}^{-1}\,s^{-1}$)	E_a ($kJ\,mol^{-1}$)
HAP	79	0.55	21	–	288	–	–
Au/HAP-H_2	81	0.41	16.2	3.7/(3.9)[d]	30	0.14	29.4
Au/HAP-O_2	83	0.42	16.5	2.9/(3.0)	14	0.25	29.2
Au/HAP-He	84	0.42	16.2	2.2/(2.3)	−10	0.08	30.4
Au/HAP-He-Re	–	–	–	2.3	–	0.15	–

[a] Average gold particle size estimated by statistic analysis from TEM results.
[b] The temperature at which the conversion was 50%.
[c] The specific reaction rate of CO oxidation under a steady state at 25 °C.
[d] Mean gold particle size of used catalyst.

carrier by deposition–precipitation with urea was characterized by several techniques including XRD, TEM, XPS, in situ DRIFTS and CO_2-TPD. Special attention is focused on the correlation between the catalytic properties and the microstructure of the metallic gold as well as the surface acid–base properties of the Au/HAP catalysts subjected to different atmospheric calcinations.

2. Experimental

2.1. Catalyst preparation

The stoichiometric HAP was prepared according to a routine wet chemical route in which HAP is precipitated from a reaction between calcium nitrate and diammonium hydrogen phosphate [34]. The solutions of $Ca(NO_3)_2{\cdot}4H_2O$ (0.5 M) and $(NH_4)_2HPO_4$ (0.3 M) were brought to pH ca. 11–12 with concentrated $NH_3{\cdot}H_2O$, respectively. The calcium solution (100 mL) was vigorously stirred at room temperature, and the phosphate solution (100 mL) was added dropwise over one hour to produce a milky precipitate which was then stirred and aged for 24 h at room temperature. The recovered precipitate was thoroughly washed (three times with distilled water and twice with ethanol), dried at 100 °C for 24 h followed by calcination in air at 600 °C for 2 h.

Gold was deposited to the as-synthesized HAP by adapting a deposition–precipitation (DP) method using urea as precipitating agent as follows: 1 g of HAP was added to 100 mL of an aqueous solution containing the desired amount of $HAuCl_4$ and urea (urea/Au = 150, molar ratio). The suspension thermostatted at 90 °C was vigorously stirred for 4 h, followed by filtering and washing several times with distilled water to remove the chlorine ($AgNO_3$ test). The resulting solid product was dried at room temperature overnight in a vacuum desiccator and then calcined in a 30 mL min^{-1} stream of He, O_2 or 5 vol% H_2 in Ar at 300 °C for 1 h. The final catalysts were stored at room temperature in a desiccator away from light. For the sake of clarity, the catalyst was referred to Au/HAP-M (see Table 1) in which M denotes the calcination atmosphere.

2.2. Catalyst characterization

The X-ray powder diffraction (XRD) measurement of the samples was carried out on a Bruker D8 Advance X-ray diffractometer using nickel filtered CuKα radiation with a voltage and current of 40 kV and 40 mA, respectively. The patterns were recorded in the range of $20^\circ \le 2\theta \le 70^\circ$ with a step size of 0.015° and a speed of 2° min^{-1}. Transmission Electron Microscopy (TEM) images were recorded on a JEOL 2011 electron microscope operating at 200 kV. Before being transferred into the TEM chamber, the samples dispersed with ethanol were deposited onto a carbon-coated copper grid and then quickly moved into the vacuum evaporator. The mean sizes of Au particles in Au/HAP samples were estimated from TEM micrographs by counting ca. 200 particles. X-ray photoelectron spectroscopy (XPS) data were recorded with a Perkin Elmer PHI 5000C system equipped with a hemispherical electron energy analyzer. The carbonaceous C 1s line (284.6 eV) was used as the reference to calibrate the binding energy (BE).

The diffuse reflectance infrared Fourier transform spectroscopy (DRIFTS) experiments were carried out on a Bruker Vector 22 FTIR spectrometer equipped with a mercury–cadmium–telluride (MCT) detector and Harrick diffuse reflectance accessory. The resolution was 4 cm^{-1} and 64 scans were taken. In situ calcination was performed with 30 mL min^{-1} of He, O_2 or 5% H_2 in Ar stream at 300 °C for 1 h, as in the case of catalyst preparation. Background signals from gas-phase CO were subtracted before the spectra were reported. The BET specific surface areas and pore size distribution of the samples were determined by adsorption–desorption of nitrogen using a Micromeritics TriStar 3000 model apparatus. Prior to the measurements all the samples were degassed at 300 °C for 12 h. Elemental analysis of the Au loading and bulk Ca/P ratio was performed using ion-coupled plasma atomic emission spectroscopy (ICP-AES) on a Thermo Electron IRIS Intrepid II XSP spectrometer.

The measurements of the basicity of the samples were conducted in a homemade apparatus using carbon dioxide (CO_2) temperature-programmed desorption (TPD) method [35]. The sample (200 mg) was purged with He flow and heated up to 450 °C at the rate of 10 °C min^{-1}, held for 60 min, then cooled down to 120 °C. The surface of the catalyst was saturated with CO_2 for an hour in this temperature, and then the excess CO_2 was purged with a He flow at 120 °C. TPD curve of the sample was measured by gas chromatography at temperatures from 120 to 500 °C with a ramp rate of 2 °C min^{-1} under He flow of 30 mL min^{-1}. The amount of desorbed CO_2 was examined by neutralization titration using an electric conductivity cell immersed in the NaOH solution [36]. CO_2 that desorbed with He was bubbled into a 0.01 mol L^{-1} NaOH aque-

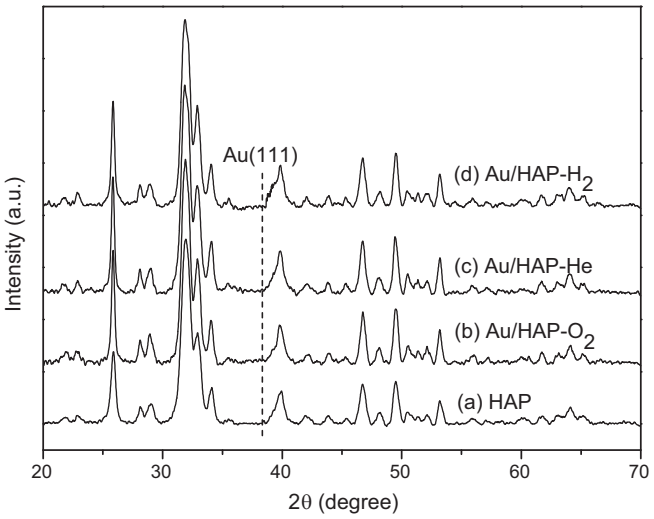

Fig. 1. XRD patterns of HAP (a) and various Au/HAP catalysts: (b) Au/HAP-O_2, (c) Au/HAP-He and (d) Au/HAP-H_2.

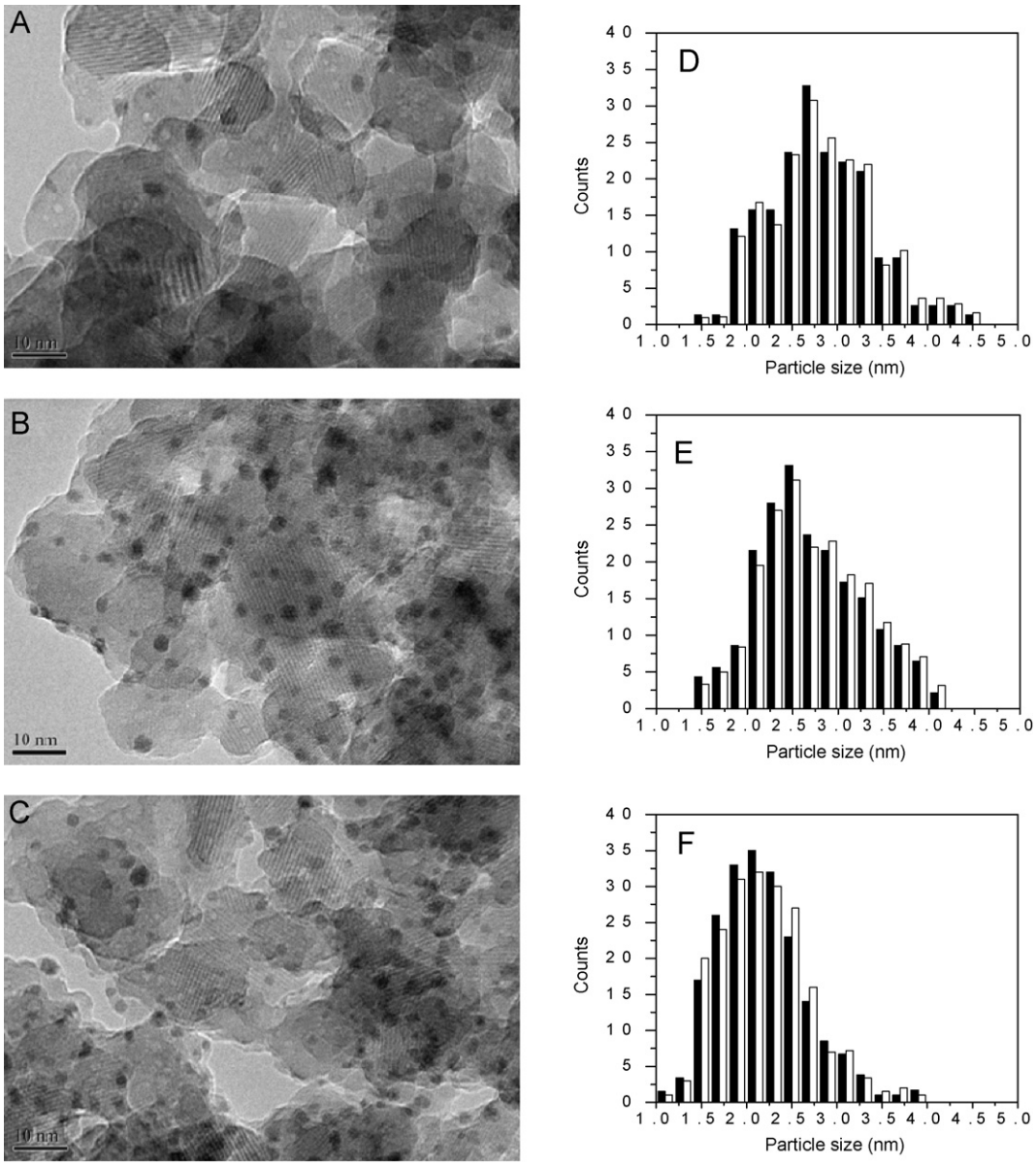

Fig. 2. TEM images of fresh samples: (a) Au/HAP-H_2, (b) Au/HAP-O_2 and (c) Au/HAP-He and size distribution of gold nanoparticles in various Au/HAP catalysts: (d) Au/HAP-H_2, (e) Au/HAP-O_2 and (f) Au/HAP-He. (■) Fresh samples, (□) after reaction.

ous solution. The amount of desorbed CO_2 was monitored from the change in conductivity of the solution. The number of basic sites is defined as the amount of substance of CO_2 molecules desorbed in the temperature range of 120–500 °C.

A home-made temperature-programmed decomposition apparatus was built according to the previous work of Stevens et al. [37]. Temperature programmed decomposition of the as-dried Au/HAP precursor (100 mg) was performed under O_2, He or 5 vol% H_2 (30 mL min^{-1}, 2 °C min^{-1} from RT to 400 °C). The gaseous compounds produced during the thermodecomposition were monitored by an on-line quadrupole mass spectrometry (OmniStar^{TM}, QMS 200). The main molecules detected were H_2O (m/e = 18), NH_3 (m/e = 17 and 15), N_2/CO (m/e = 28), and N_2O/CO_2 (m/e = 44) [38,39].

2.3. CO oxidation and kinetic measurements

The catalytic activity test for CO oxidation was evaluated at atmospheric pressure using a fixed bed quartz reactor (i.d. 3 mm). The weight of the catalyst was 30 mg, and the total flow rate of the reaction gas was 50 mL min^{-1}, with a composition of 1%CO–20%O_2 (balanced with He). Kinetic measurements were performed under different reaction conditions, with typically about 5–15 mg catalyst powder. To limit the conversion to values typically below 25%, the catalysts were diluted with chemically inert α-Al_2O_3. The reactions were carried out with 100 mL min^{-1} of 1%CO–20%O_2 balanced with He. Kinetic data were collected after 90-min reaction. The composition of the influent and effluent gas was detected with an online gas chromatograph (TCD) equipped with a TDX-01 column. The conversion of CO was calculated from the change in CO concentrations of the inlet and outlet gases.

3. Results and discussion

3.1. Structural properties and chemical states

The real gold contents of various Au/HAP catalysts were determined by ICP-AES. The measured gold content, 2.9 wt%, was

Table 2
XPS results of various Au/HAP catalysts calcined under different atmospheres.

Catalysts	B.E. of Au $4f_{7/2}$ (eV)	$Au^{\delta+}$ (%)	B.E. of Ca $2p_{3/2}$ (eV)	B.E. of P $2p_{3/2}$ (eV)	Ca/P	Au/Ca
HAP	–	–	346.8	132.6	1.48	–
Au/HAP-H_2	83.9	2.8	346.8	132.6	1.33	0.108
Au/HAP-O_2	84.1	15.7	346.7	132.7	1.29	0.124
Au/HAP-He	84.0	9.1	346.7	132.7	1.39	0.169
Au/HAP-He-Re	84.0	11.8	346.7	132.7	1.37	0.167

essentially the same as the nominal loading (3 wt%) for all samples, confirming the effectiveness of the urea-mediated Au deposition onto the HAP support [40]. The textural properties of the as-synthesized HAP sample and various Au/HAP catalysts are reported in Table 1. The specific surface area (S_{BET}) and the cumulative pore volume of the parent HAP sample have been measured to be 79 $m^2\,g^{-1}$ and 0.55 $cm^3\,g^{-1}$, respectively (shown in Table 1). The pore size distribution measurements show that a well-developed mesostructure was achieved for the HAP sample, which exhibits a narrow pore size distribution in the range of 15–30 nm (not shown). When gold was deposited onto the surface of HAP, a slightly increased BET surface area was identified, as opposed to the variation trend being observed for the corresponding sample pore volume and average pore size distribution. It is interesting to note that the decreased pore size and pore volume suggests that gold nanoparticles are entrapped in the mesoporous matrix of the HAP material, while the slightly enhanced BET surface area is most likely due to the much larger surface area of the as-deposited small gold nanoparticles [41]. The specific surface areas are 84, 83 and 81 $m^2\,g^{-1}$ for Au/HAP-He, Au/HAP-O_2 and Au/HAP-H_2 catalysts, respectively. The calcination atmosphere, however, was found to have little influence on the textural data among the Au-containing samples.

The XRD pattern of the as-synthesized HAP support (Fig. 1(a)) shows well-defined diffraction feature characteristics of pure apatite (JCPDS no. 9-432). After the deposition of Au nanoparticles onto the HAP support, an almost identical XRD pattern was obtained for Au/HAP comparing with HAP, indicating that the crystal structure of the HAP support was well maintained. Fig. 1(b)–(d) shows the XRD patterns for various Au/HAP catalysts. Comparison with the XRD pattern of HAP reveals that most of the reflections stem from the parent support material. No distinct metallic Au ($2\theta = 38.2^\circ$) reflections are visible in the XRD patterns of any samples, owing to the fact that the gold particle sizes are very small. TEM was then used as a complementary technique to examine the structures of gold particles. Representative TEM images for the fresh catalysts are shown in Fig. 2(a)–(c). The average gold particle size is estimated to be ca. 2.2, 2.9 and 3.7 nm for the samples calcinated in He, O_2 and H_2 atmospheres, respectively (see Table 1), which clearly indicates that the calcination environment has an influence on the gold particle size. Such a calcination-atmosphere dependent phenomenon was also observed for titania supported gold catalysts prepared by urea-DP method [42,43]. After the ambient temperature CO oxidation reaction, the mean particle size hardly increased (see Fig. 2(d)–(f) and Table 1). Apparently, the low reaction temperature was too low for pronounced particle growth. This also agrees well with previous observations of a much lesser gold particle growth when calcinated under lower temperatures [14,44]. TEM measurement was also performed on the regenerated Au/HAP-He catalyst (not shown). It is interesting to find the average particle size did not increase either (see Table 1).

XPS characterization was performed to investigate the chemical states of various Au/HAP catalysts. The Au 4f XPS spectra of all relevant samples are presented in Fig. 3(a)–(d). The detailed XPS results are summarized in Table 2. Quantitative deconvolution of the Au 4f peaks revealed ca. 15.7% contribution from partially oxidized Au species (86.0 eV) for O_2-treated sample and the amount of positively charged gold species in the three fresh samples decreased in the following order: Au/HAP-O_2 > Au/HAP-He > Au/HAP-H_2 (see Table 2). This indicates that calcination in reductive atmosphere can lead to formation of higher fraction of metallic gold (Au^0). However, different atmospheres had a negligible effect on the binding energies of Ca $2p_{3/2}$ and P $2p_{3/2}$ (spectra not shown for brevity). It may be noted that the high vacuum required for XPS and the energy of the X-rays could lead to the reduction of a fraction of positively charged gold species. Therefore, the real percentages of the fraction of cationic gold species that are present before analysis may be underestimated by XPS. The surface composition in Table 2 shows that the calcination of catalyst precursor under H_2 atmosphere resulted in the smallest Au/Ca molar ratio. The ratio of Au/Ca of the three as-calcined samples increased in the following order: Au/HAP-H_2 < Au/HAP-O_2 < Au/HAP-He (see Table 2), in line with the TEM results revealing that calcination in an inert atmosphere favors a formation of the smallest Au nanoparticles over the HAP support.

3.2. CO oxidation activity, reaction kinetics and stability

The catalytic performances of various Au/HAP catalysts in CO oxidation are shown in Fig. 4(a), where the CO conversion is reported as a function of temperature (light-off test). For the sake

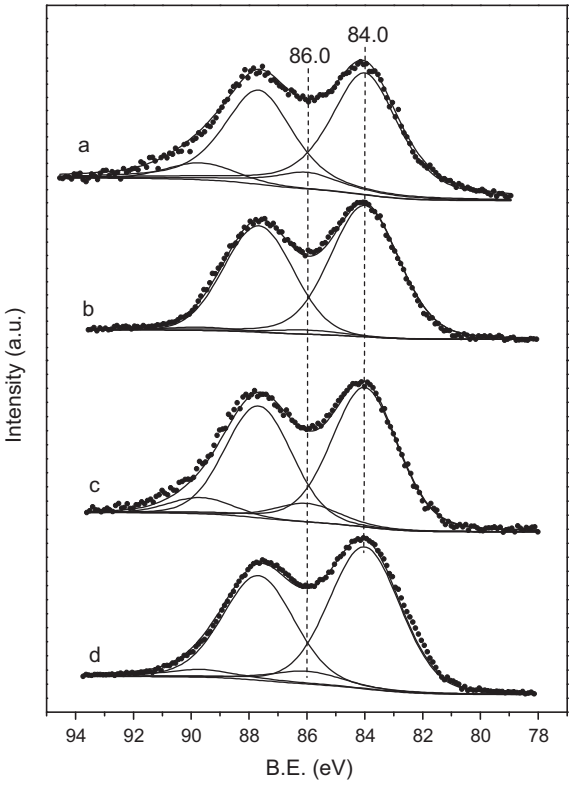

Fig. 3. Au 4f XPS spectra of various Au/HAP catalysts: (a) Au/HAP-O_2, (b) Au/HAP-H_2, (c) Au/HAP-He-Re and (d) Au/HAP-He.

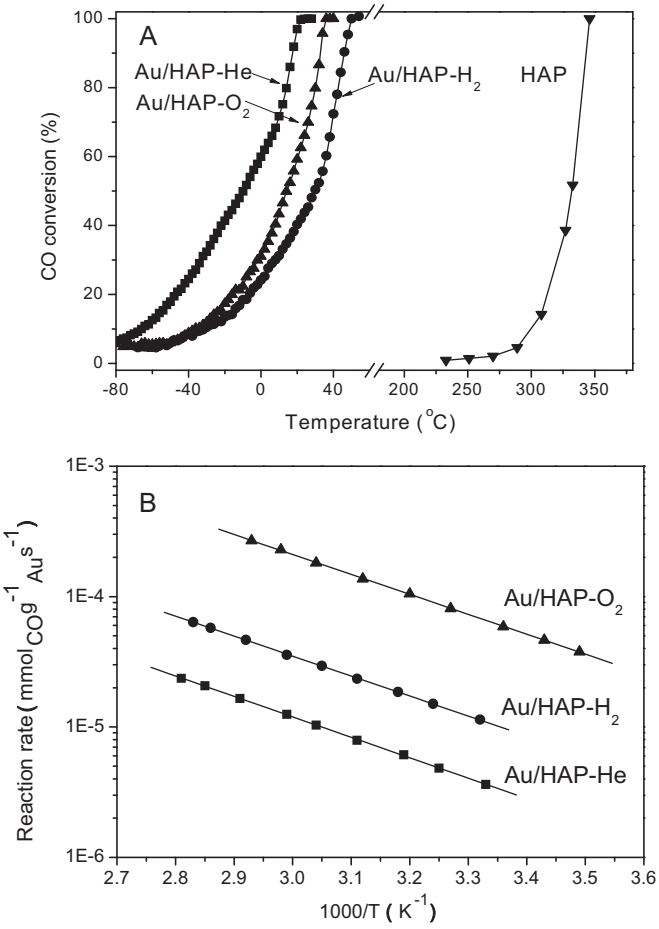

Fig. 4. (a) CO oxidation activity of Au/HAP catalysts calcined under different atmospheres. Reaction conditions: 30 mg catalyst, 1%CO–20%O_2 balanced with He, 50 mL min^{-1}. (b) Arrhenius plots of the reaction rate vs. 1/T for CO oxidation over various Au/HAP catalysts. Reaction conditions: 5–15 mg catalyst, 1%CO–20%O_2 balanced with He, 100 mL min^{-1}.

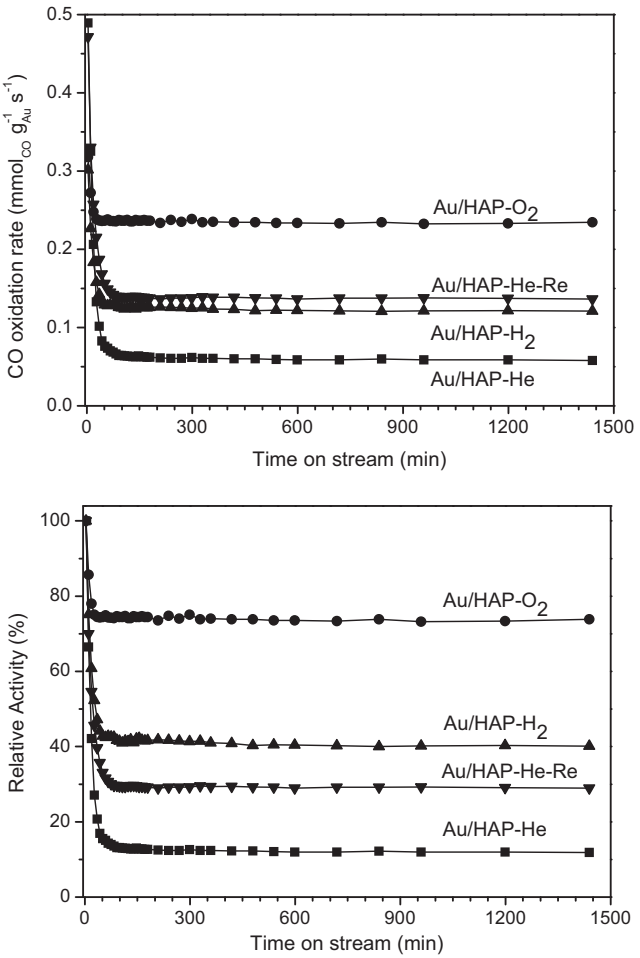

Fig. 5. Evolution of the mass specific CO oxidation rate (a) and the relative activity (b) on differently calcined Au/HAP catalysts for 24 h on stream. Reaction conditions: 30 mg catalyst, 25 °C, 1%CO–20%O_2 balanced with He, 50 mL min^{-1}. Au/HAP-He-Re refers to Au/HAP-He after regeneration.

of comparison, the activity of parent HAP is also included. It is clear that the activities of the supported gold catalysts are much higher than that for the pure HAP support material. Moreover, it is seen that the light-off activity of Au/HAP is highly sensitive to the calcination atmosphere. Of all Au/HAP catalysts investigated, Au/HAP-He shows the highest light-off activity for CO oxidation. The temperature at which the conversion was 50% (T_{50}) for Au/HAP-He is −10 °C (see Table 1), ca. 40 °C below that for Au/HAP-H_2. It is worthwhile to note that complete oxidation of CO could be attained at sub-ambient temperature over Au/HAP-He, conditions under which the previously reported HAP foams [32] or carbonated HAP [33] supported gold catalysts were much less effective for this reaction. On the other hand, kinetic studies showed that all catalysts have similar activation energies (E_a), as reflected by the Arrhenius plots presented in Fig. 4(b). This result suggests that different calcination atmospheres do not change the reaction mechanism of CO oxidation over the Au/HAP. It is also interesting to note that in contrast to light-off test obtained from Fig. 4(a), the oxidative calcination gave the highest activity in terms of the reaction rates at steady state (after 90 min reaction, Fig. 4(b)).

Fig. 5 illustrates the deactivation of the various Au/HAP catalysts at 25 °C during 24 h of CO oxidation reaction. The activities in Fig. 5(a) are described by the mass specific rate under similar reaction condition. Fig. 5(b) shows the deactivation on a relative scale, relative to an initial activity of 100%. The oxidative calcination-derived Au/HAP-O_2 shows the best stability among the studied catalysts, with activity decayed by 27% after 24 h on stream. In contrast, the most severe deactivation occurred on Au/HAP-He calcined under inert conditions, with loss of activity by 88% during the same period. The deactivated catalyst was then regenerated in He stream (with the same condition as that for the catalyst preparation) with largely restored initial activity. Interestingly, the stability of the regenerated Au/HAP-He was prominently improved, with activity decayed by 71% after 24-h reaction. As for the catalyst precursor calcined in reductive H_2, a rapid deactivation was observed in the initial 40 min. However, the deactivation rate slowed down significantly afterwards, and the activity loss for Au/HAP-H_2 was 60% in 24 h. It turns out that the steady-state activity follows the decreasing order of Au/HAP-O_2 > Au/HAP-H_2 > Au/HAP-He (Fig. 4(b) and Fig. 5(a)).

3.3. *In situ DRIFTS measurements*

To better understand the origin of the different catalytic behaviors with various calcinations, the surface nature of the samples has been studied by DRIFTS, a powerful technique that can provide valuable insights into the mechanism of heterogeneous catalytic reactions, especially under in situ conditions [45]. In this work, CO adsorption on differently calcinated Au/HAP catalysts and the further evolution of reaction intermediates along with side products during CO oxidation were also investigated.

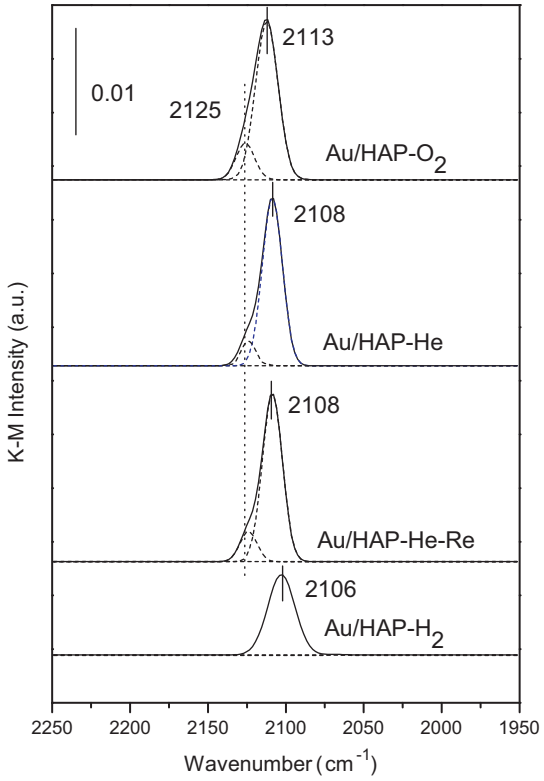

Fig. 6. DRIFT spectra of CO adsorption on various Au/HAP catalysts after CO adsorption for 3 min.

3.3.1. CO adsorption studies

Fig. 6 shows the DRIFT spectra for CO adsorption on various catalysts after in situ calcination under different atmospheres. The adsorption of CO on Au/HAP-O_2 for 3 min resulted in a strong band at ca. 2113 cm^{-1} with a small shoulder at higher frequency of ca. 2125 cm^{-1}. The former band is generally attributed to CO adsorption on the step/kink defect sites of the supported gold nanoparticles (Au^0–CO) [35], while the latter is associated with CO adsorption on positively polarized gold species (O–$Au^{\delta+}$–CO), which most likely result from the spillover of oxygen or OH groups from the support onto the Au nanoparticles [46]. Such CO adsorption bands have also been observed on the Au/TiO_2 [44] and Au/α-Mn_2O_3 [18] catalysts under similar conditions.

As compared with the O_2-calcinated sample, the Au^0–CO band is slightly stronger on Au/HAP-He. This observation indicates the presence of more defective gold sites on the He-calcinated sample. CO adsorption was also performed on the regenerated Au/HAP-He. It is interesting to find that the intensity of the O–$Au^{\delta+}$–CO band increased, with that of the Au^0–CO band almost unaltered as compared with that of the fresh Au/HAP-He. An increase in the positively charged gold sites can be rationalized by the fact that excess oxygen is present under reaction conditions. The Au/HAP-H_2 sample shows the weakest CO adsorption band at 2106 cm^{-1}. It turns out that the strength of CO adsorption follows the decreasing order of Au/HAP-He > Au/HAP-O_2 > Au/HAP-H_2, but the wavenumber of the CO adsorption peak follows the increasing order of Au/HAP-H_2 < Au/HAP-He < Au/HAP-O_2. These results indicated that calcination atmosphere have a pronounced effect on the electronic structure of Au particles loaded on the HAP support.

3.3.2. State of the catalysts during CO oxidation reaction

The accumulation of adsorbed surface species on various catalysts during CO oxidation reaction was also followed by in situ DRIFTS measurements. Fig. 7(a) illustrates the evolution of the full spectra recorded on Au/HAP-O_2 during the reaction, with the enlarged details of the CO/CO_2 and carbonate regions being presented in Fig. 7(b)–(d). The spectra reveal the characteristic peaks of Au^0–CO at 2113 cm^{-1}, the bands of gaseous CO_2 at 2342 and 2358 cm^{-1} and a set of broad bands in the range of 1300–1700 cm^{-1}. The bands at 1682, 1368, 1611 and 1436 cm^{-1} are commonly assigned to the C=O, asymmetric O–C–O stretch vibration of bidentate carbonates, the symmetric and asymmetric O–C–O stretch vibration of monodentate carbonates [18], respectively. It is important to remark that the general features were similar for all samples, while the characteristic frequencies and the intensities as well as their evolution during reaction were appreciably different. For instance, the CO related peaks appear at 2106 and 2108 cm^{-1} on the Au/HAP-H_2 and Au/HAP-He catalysts, respectively. In all cases, over the investigated time scale, the location of the Au^0–CO peak remains constant. Moreover, the general shapes of CO/CO_2 related peaks did not change with time, indicating that the nature of adsorbed CO species and thus of the adsorption sites were not modified by the reaction.

The integrated intensity of CO, CO_2 and carbonate-related peaks for various Au/HAP samples are plotted as a function of time as shown in Fig. 8. The CO, CO_2 and carbonate-related peaks for each sample increased significantly during the first few minutes and then slowly approached a steady state. It is worthy to note that the intensity of the CO and CO_2 related peaks for Au/HAP-O_2 was much stronger than that of Au/HAP-H_2. Meanwhile, the weakest CO and CO_2 adsorption peaks were found on Au/HAP-He. As for the carbonate peak evolution, the intensity (after 90 min reaction) decreases in the order of Au/HAP-He > Au/HAP-H_2 > Au/HAP-O_2. In general, the evolution trend of the intensity closely resembled that of the deactivation curve as described above.

3.4. Discussion

Results obtained in this study clearly demonstrate that the calcination atmosphere has a significant influence on both structural and catalytic properties of the Au/HAP system in ambient CO oxidation. Calcination in an inert atmosphere, i.e., He, leads to a gold catalyst with the highest initial activity, which however suffers the most severe deactivation with time on stream. In contrast, oxidative calcination affords the most stable catalyst while maintaining high activity. The trend of the initial activity for differently calcinated catalysts follows the order of Au/HAP-He > Au/HAP-O_2 > Au/HAP-H_2, which is correlated to the particle size of gold. TEM images revealed the apparently different average sizes of the gold particles under various calcination conditions and XPS results suggested the highest surface Au/Ca ratio on Au/HAP-He catalyst among the three samples. It is generally accepted that the amount of low-coordinated Au atoms, the key sites for the adsorption and activation of CO, depends strongly on the size of gold nanoparticles [47]. Boccuzzi et al. pointed out that adsorption of CO on gold exhibits a size effect in that small particles adsorb CO more strongly [47]. In the present work, from the IR spectra of CO adsorption on the Au/HAP catalysts, as shown in Fig. 6, the CO adsorption peak is much stronger on inert or oxidative- calcination derived Au/HAP samples, indicating more exposure of defective gold sites with respective to the Au/HAP-H_2 sample. This fact may account for the lowest initial activity of Au/HAP-H_2 and explain the highest initial activity of Au/HAP-He.

It is generally accepted that two main factors may contribute to the deactivation of Au catalysts in CO oxidation, i.e., the growth of gold particle size induced by the exothermic nature of the reaction and the accumulation of carbonates blocking the active sites [48–53]. For gold catalysts with very small particle size (ca. 2–5 nm) the problem of particle stability is expected to be an issue of particular concern, supposedly due to the low Tammann temperature of

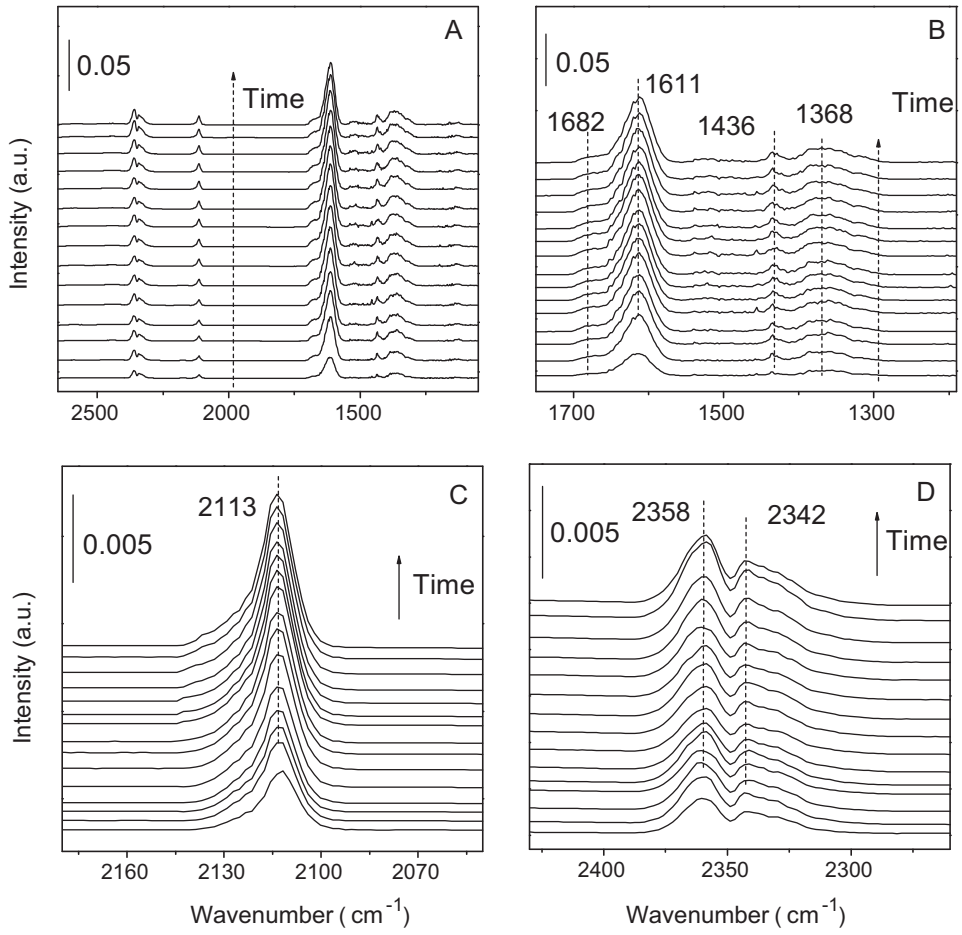

Fig. 7. Sequence of in situ DRIFT spectra recorded during CO oxidation on Au/HAP-O_2 (reaction times: 1, 3, 5, 8, 11, 19, 27, 35, 43, 51, 59, 67, 75, 83, 91 min). (a) full spectra, (b) enlarged details of the carbonate region, (C) enlarged details of the region characteristic for CO adsorption and (D) enlarged details of the C=O stretch region characteristic for CO_2 adsorption.

gold (395 °C) [54]. As a typical example, growth of metal particles by sintering readily occurred with model catalysts (Au/TiO_2(1 1 0) [48], Au/SiO_2/Si(1 0 0) [49]), which was usually taken as the main reason leading to the deactivation of these systems. In contrast, no pronounced particle growth has been observed with 'real' catalysts such as Au/TiO_2 [50,55], and Au/Al_2O_3 [20,21], possibly due to the presence of a strong metal–support interaction (SMSI) between the gold particles and the surface of the underlying support. At this juncture, it is worthwhile to point out that the reaction-induced increase of the gold particle size is negligible based on the TEM analysis (see Fig. 2), despite a very small Au particle size in the range of 2–4 nm being identified for all Au/HAP samples. As noted above, both the specific surface feature of the HAP support and the mild reaction conditions could play a role in stabilizing the gold particles in the Au/HAP system. Therefore, gold particle growth over the Au/HAP catalysts can be ruled out as main origin for the deactivation.

Recently, on investigating the effect of reaction atmospheres on the catalytic performance of a set of unconditioned Au/TiO_2 catalysts, Denkwitz et al. suggested that the dominant reason for the deactivation of Au/TiO_2 is not due to the reaction-induced growth of the very small Au particles (ca. 1.3–1.8 nm), but rather the buildup of surface carbonates on the support during reaction [50]. Conversely, by monitoring the deactivation behavior of a moderately O_2-pretreated Au/α-Mn_2O_3 catalyst, we have very recently shown by in situ DRIFTS that the rapid accumulation of surface carbonate species is not in line with the superior stability of the O_2-Au/α-Mn_2O_3 sample [18]. The reason of this effect has been rationalized as the favorable formation of an oxygen-rich Au-support interface being particularly active for CO oxidation. As for the differently calcined Au/HAP catalysts in the present study, investigation by means of in situ DRIFTS clearly shows that substantial amount of surface carbonate species is produced during the reaction, especially for the Au/HAP-He and Au/HAP-H_2 catalysts (Fig. 8(c)). In this context, the rapid deactivation of the Au/HAP-He catalyst can be well understood by the continuous accumulation of carbonate-like species. Moreover, it is noteworthy that the deactivated Au/HAP-He catalyst could be regenerated to a large extent along with an even improved stability. All these results strongly suggest that carbonate accumulation plays a crucial role in controlling the deactivation behavior of the Au/HAP catalyst.

To gain a further insight into the catalyst stability in relation to carbonate accumulation on these samples, the surface basicity properties of various catalysts have been investigated. HAP has attracted considerable recent attention as an acid or base catalyst because of its unusual property of containing both acid sites and basic sites in a single crystal lattice [29]. It is known that the bulk Ca/P ratio has an important influence on the acid–base property of this material. For example, at a relatively lower Ca/P ratio of 1.50, highly crystalline HAP acts as an acid catalyst, catalyzing mainly ethylene synthesis from ethanol by dehydration [56]; however, at a stoichiometric Ca/P ratio of 1.67, it acts as a basic catalyst, catalyzing chiefly acetaldehyde synthesis from ethanol by dehydrogenation [56]. It is evident that in the present case the surface Ca/P ratio (Table 2) as revealed by XPS for various Au/HAP catalysts is considerably lower than that of the blank HAP, inferring

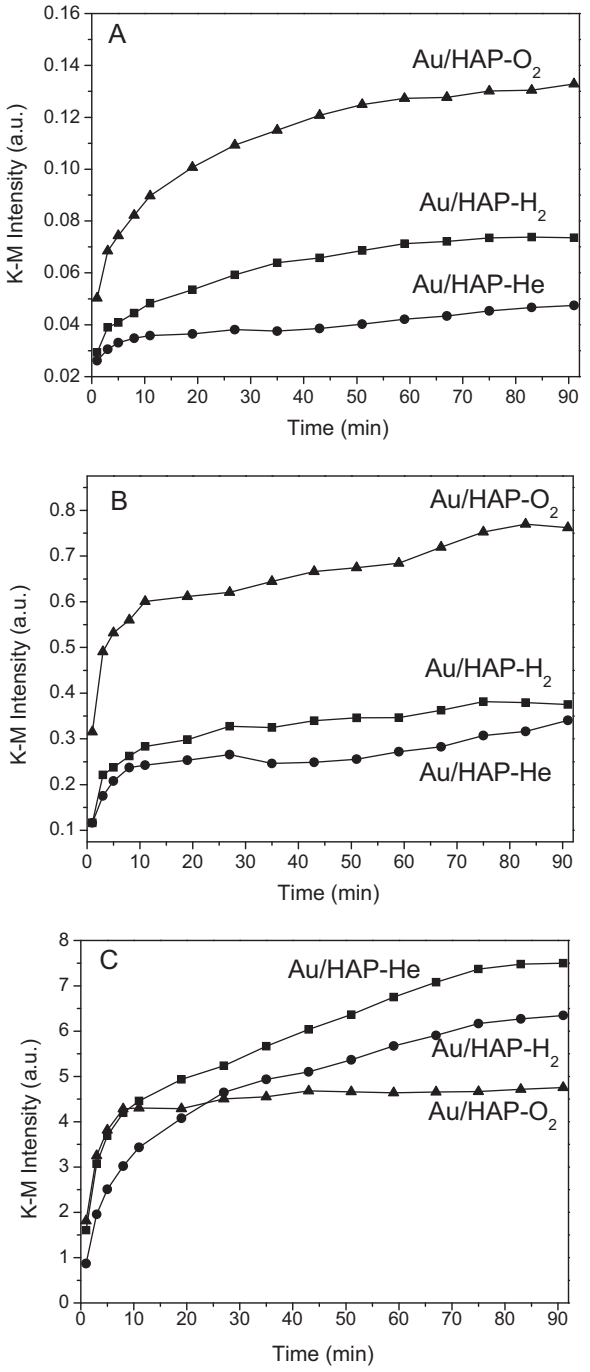

Fig. 8. Evolution of the DRIFT signals characteristic for (a) CO adsorption, (b) CO_2 and (c) carbonate species as function of time during CO oxidation.

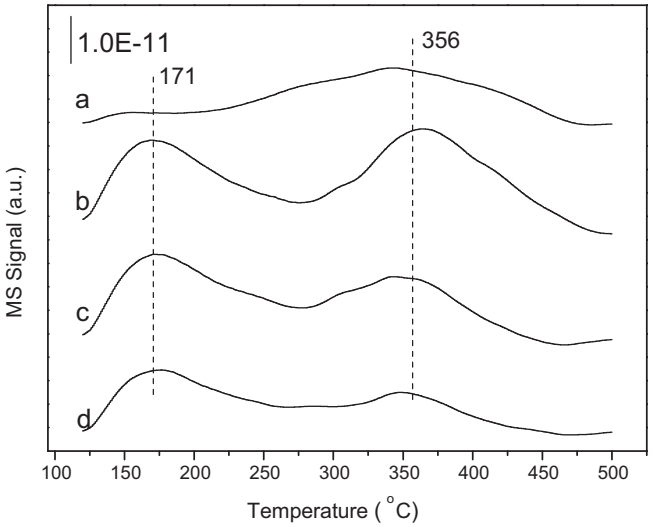

Fig. 9. CO_2-TPD curves of various samples. (a) HAP, (b) Au/HAP-He, (c) Au/HAP-H_2 and (d) Au/HAP-O_2.

a strong modification of the acid–base properties of the HAP support upon Au introduction. Taking into account the fact that the Au/HAP-He sample has the highest surface Ca/P ratio, one might envisage that the calcination in inert atmosphere can resulted in a higher population of surface basic sites over the HAP support. To testify this hypothesis, the CO_2-TPD of the various Au/HAP samples was conducted (Fig. 9). The results given in Table 3 show that the variation in the overall surface basicity of the various Au/HAP catalysts is consistent with the evolution rate of the absorption bands corresponding to carbonate species as reflected by the in situ DRIFT studies. This scenario, in conjunction with the fact that the activity of the deactivated Au/HAP-He can be largely restored by re-calcination in He atmosphere, suggests the essential role of surface basicity in dominating the deactivation of the Au/HAP catalysts.

Having established that the calcination atmosphere has a pronounced influence on the surface nature and catalytic properties of the Au/HAP system for CO oxidation, it is of interest to clarify the possible role of calcination atmosphere that may be responsible for the observed differences in the surface basicity. To this end, a temperature-programmed decomposition of the as-dried Au/HAP precursor under flowing oxygen (O_2), helium (He) and hydrogen (H_2/Ar) was conducted, and the corresponding signals of evolved species were collected in Fig. 10. Recently, on investigating the elemental composition of gold species deposited onto the TiO_2 surface prepared by deposition–precipitation with urea, Zanella et al. have shown by combined EXAFS, XANES and elemental analysis that the supported gold compound could be described as $AuN_{2.2}O_{1.2}C_{0.9}H_{4.2}Cl_{0.1}$ [57]. Later, the same authors also revealed that calcination atmosphere has a great influence on the particle size of the final Au/TiO_2 catalyst [43]. It is evident that the

Table 3
Surface basicity properties of various catalysts.

Catalysts	CO_2 uptake[a] (mmol g^{-1})		Total CO_2 uptake[a] (mmol g^{-1})	Accumulation of carbonates (K-M Intensity (a.u.))[b]
	Weak basic sites	Moderate basic sites		
HAP	0.08	0.25	0.33	–
Au/HAP-O_2	0.23	0.15	0.38	4.8
Au/HAP-H_2	0.26	0.30	0.56	6.3
Au/HAP-He	0.29	0.41	0.70	7.5

[a] Calculated from temperature-programmed desorption of CO_2.
[b] Estimated from the carbonate intensity after 90 min of the reaction as shown in Fig. 8(C).

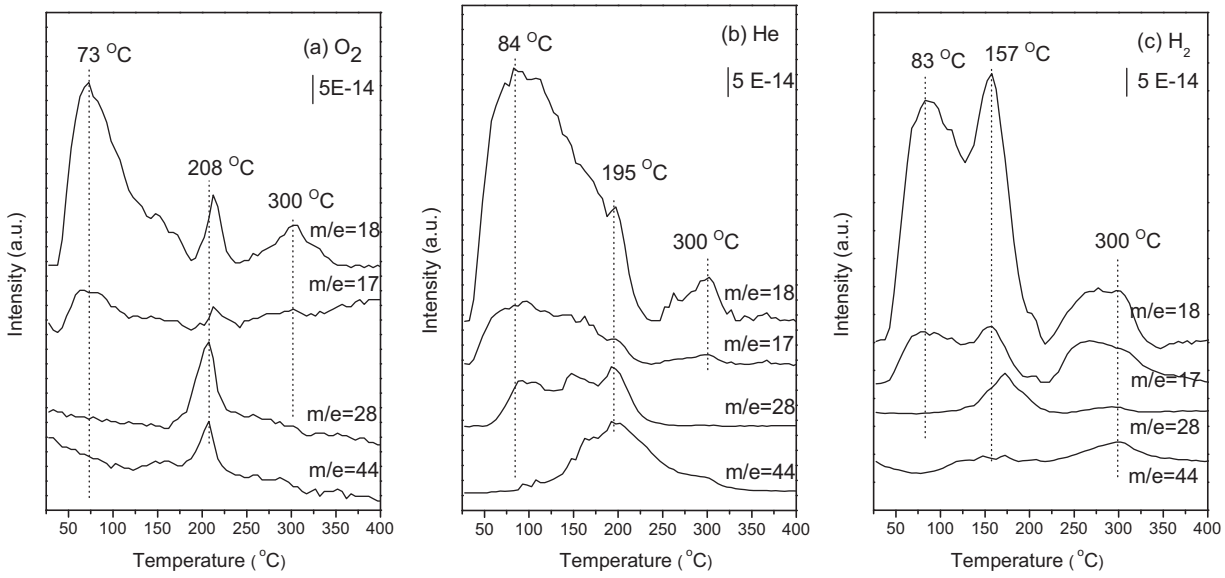

Fig. 10. Temperature-programmed decomposition of the as-dried Au/HAP precursor under different atmospheres: (a) O_2, (B) He, (c) 5 vol% H_2/Ar.

thermo-evolution data as reported in Fig. 10 indicate that the decomposition of $AuN_{2.2}O_{1.2}C_{0.9}H_{4.2}Cl_{0.1}$ species to produce metallic Au^0 supported on HAP proceeds much more rapidly under oxidative atmosphere, inferring a strong atmosphere-dependence of the precursor activation process. Taking into account that the as-deposited $AuN_{2.2}O_{1.2}C_{0.9}H_{4.2}Cl_{0.1}$ compound may have a strong interaction with the underlying HAP support, it is reasonable that the varied surface nature of the Au/HAP system arises largely from the pretreatment-dependent decomposition behavior of the supported $AuN_{2.2}O_{1.2}C_{0.9}H_{4.2}Cl_{0.1}$ precursor.

4. Conclusions

In this study, the effect of the calcination atmosphere on the structural and catalytic properties of the Au/HAP system in the ambient CO oxidation reaction was investigated. The results showed that the calcination atmosphere affected greatly the Au/HAP catalysts in many ways including surface acid–base properties, the microstructure of the metallic gold and the metal–support interaction, which are related to their catalytic behaviors. After an inert He calcination, the Au/HAP-He catalyst attained the highest initial activity, which however suffered the most drastic deactivation with time on stream. When calcinated in an oxidative O_2 atmosphere, the Au/HAP-O_2 catalyst displayed the best stability thus affording the highest steady-state activity among the three samples. TEM results revealed that Au/HAP-He had the smallest Au particle size which may play a key role in attaining high initial activity. As compared with the inertly and reductively calcinated samples, the superior stability of Au/HAP-O_2 has been attributed to its limited surface basicity as revealed by the CO_2-TPD and in situ DRIFTS studies.

Acknowledgments

This work was financially supported by the National Natural Science Foundation of China (20633030, 20721063, 20873026, 21073042), the National Basic Research Program of China (2009CB623506), New Century Excellent Talents in the University of China (NCET-09-0305) and Science & Technology Commission of Shanghai Municipality (08DZ2270500).

References

[1] A.J. Dyakonov, C.A. Little, Appl. Catal. B 67 (2006) 52–59.
[2] M. Haruta, T. Kobayashi, H. Sano, N. Yamada, Chem. Lett. 2 (1987) 405–408.
[3] L. Ilieva, G. Pantaleo, J.W. Sobczak, I. Ivanov, A.M. Venezia, D. Andreeva, Appl. Catal. B 76 (2007) 107–114.
[4] I. Dobrosz-Gómez, I. Kocemba, J.M. Rynkowski, Appl. Catal. B 88 (2009) 83–97.
[5] G.C. Bond, D.T. Thompson, Catal. Rev. Sci. Eng. 41 (1999) 319–388.
[6] A.S.K. Hashmi, G.J. Hutchings, Angew. Chem. Int. Ed. 45 (2006) 7896–7937.
[7] F.S. Stone, Adv. Catal. 13 (1962) 1–50.
[8] A.S. Ivanova, E.M. Slavinskaya, R.V. Gulyaev, V.I. Zaikovskii, O.A. Stonkus, I.G. Danilova, L.M. Plyasova, I.A. Polukhina, A.I. Boronina, Appl. Catal. B 97 (2010) 57–71.
[9] M. Haruta, Chem. Rec. 3 (2003) 75–87.
[10] M. Haruta, M. Daté, Appl. Catal. A 222 (2001) 427–437.
[11] M. Haruta, S. Tsubota, T. Kobayashi, H. Kageyama, M.J. Genet, B. Delmon, J. Catal. 144 (1993) 175–192.
[12] M.C. Raphulu, J. McPherson, E. van der Lingen, J.A. Anderson, M.S. Scurrell, Gold Bull. 43 (2010) 21–27.
[13] A. Karpenko, R. Leppelt, J. Cai, V. Plzak, A. Chuvilin, U. Kaiser, R.J. Behm, J. Catal. 250 (2007) 139–150.
[14] B. Schumacher, V. Plzak, M. Kinne, R.J. Behm, Catal. Lett. 89 (2003) 109–114.
[15] F. Moreau, G.C. Bond, A.O. Taylor, J. Catal. 231 (2005) 105–114.
[16] N. Lopez, T.V.W. Janssens, B.S. Clausen, Y. Xu, M. Mavrikakis, T. Bligaard, J.K. Nørskov, J. Catal. 223 (2004) 232–235.
[17] E.D. Park, J.S. Lee, J. Catal. 186 (1999) 1–11.
[18] L.C. Wang, L. He, Y.M. Liu, Y. Cao, H.Y. He, K.N. Fan, J.H. Zhuang, J. Catal. 264 (2009) 145–153.
[19] K.Y. Ho, K.L. Yeung, J. Catal. 242 (2006) 131–141.
[20] C.K. Costello, M.C. Kung, H.-S. Oh, Y. Wang, H.H. Kung, Appl. Catal. A 232 (2002) 159–168.
[21] C.K. Costello, J.H. Yang, H.Y. Law, Y. Wang, J.-N. Lin, L.D. Marks, M.C. Kung, H.H. Kung, Appl. Catal. A 243 (2003) 15–24.
[22] M. Comotti, W.C. Li, B. Spliethoff, F. Schüth, J. Am. Chem. Soc. 128 (2006) 917–924.
[23] N.F. Zheng, G.D. Stucky, J. Am. Chem. Soc. 128 (2006) 14278–14280.
[24] D.W. Goodman, Catal. Lett. 99 (2005) 1–4.
[25] M.J. Li, Z.L. Wu, Z. Ma, V. Schwartz, D.R. Mullins, S. Dai, S.H. Overbury, J. Catal. 266 (2009) 98–105.
[26] W.F. Yan, S. Brown, Z.W. Pan, S.M. Mahurin, S.H. Overbury, S. Dai, Angew. Chem. Int. Ed. 45 (2006) 3614–3618.
[27] H.L. Lian, M.J. Jia, W.C. Pan, Y. Li, W.X. Zhang, D.Z. Jiang, Catal. Commun. 6 (2005) 47–51.
[28] J.C. Elliot, Structure and Chemistry of the Apatites and Other Calcium Orthophosphates, Elsevier, Amsterdam, 1994.
[29] Z. Opre, D. Ferri, F. Krumeich, T. Mallat, A. Baiker, J. Catal. 251 (2007) 48–58.
[30] H. Sun, F.Z. Su, J. Ni, Y. Cao, H.Y. He, K.N. Fan, Angew. Chem. Int. Ed. 48 (2009) 4390–4393.
[31] A. Venugopal, M.S. Scurrell, Appl. Catal. A 245 (2003) 137–147.
[32] N. Phonthammachai, Z.Y. Zhong, J. Guo, Y.F. Han, T.J. White, Gold Bull. 41 (2008) 42–50.
[33] M.I. Domínguez, F. Romero-Sarria, M.A. Centeno, J.A. Odriozola, Appl. Catal. B 87 (2009) 245–251.
[34] S. Sugiyama, T. Minami, H. Hayashi, M. Tanaka, N. Shigemoto, J.B. Moffat, J. Chem. Soc. Faraday Trans. 92 (1996) 293–299.

[35] N.S. Resende, M. Nele, V.M.M. Salim, Thermochim. Acta 451 (2006) 16–21.
[36] S. Sato, R. Takahashi, M. Kobune, H. Gotoh, Appl. Catal. A 356 (2009) 57–63.
[37] R.W. Stevens Jr., S.S.C. Chuang, B.H. Davis, Thermochim. Acta 407 (2003) 61–71.
[38] L. Delannoy, N.E. Hassan, A. Musi, N.N. Le To, J.-M. Krafft, C. Louis, J. Phys. Chem. B 110 (2006) 22471–22478.
[39] A. Goguet, D. Schweich, J.-P. Candy, J. Catal. 220 (2003) 280–290.
[40] R. Zanella, S. Giorgio, C.R. Henry, C. Louis, J. Phys. Chem. B 106 (2002) 7634–7642.
[41] Y. Jin, P.J. Wang, D.H. Yin, J.F. Liu, H.Y. Qiu, N.Y. Yu, Microporos. Mesopor. Mater. 111 (2008) 569–576.
[42] S. Tsubota, D.A.H. Cunningham, Y. Bando, M. Haruta, Stud. Surf. Sci. Catal. 91 (1995) 227–235.
[43] R. Zanella, C. Louis, Catal. Today 107–108 (2005) 768–777.
[44] F. Boccuzzi, A. Chiorino, M. Manzoli, P. Lu, T. Akita, S. Ichikawa, M. Haruta, J. Catal. 202 (2001) 256–267.
[45] A. Chiorino, M. Manzoli, F. Menegazzo, M. Signoretto, F. Vindigni, F. Pinna, F. Boccuzzi, J. Catal. 262 (2009) 169–176.
[46] F. Boccuzzi, A. Chiorino, M. Manzoli, Surf. Sci. 454–456 (2000) 942–946.
[47] F. Boccuzzi, A. Chiorino, M. Manzoli, Mater. Sci. Eng. C 15 (2001) 215–217.
[48] M. Valden, X. Lai, D.W. Goodman, Science 281 (1998) 1647–1650.
[49] L. Guczi, G. Petö, A. Beck, K. Frey, O. Geszti, G. Molnár, C. Daróczi, J. Am. Chem. Soc. 125 (2003) 4332–4337.
[50] Y. Denkwitz, Z. Zhao, U. Hörmann, U. Kaiser, V. Plzak, R.J. Behm, J. Catal. 251 (2007) 363–373.
[51] P. Konova, A. Naydenov, Cv. Venkov, D. Mehandjiev, D. Andreeva, T. Tabakova, J. Mol. Catal. A 213 (2004) 235–240.
[52] P. Konova, A. Naydenov, T. Tabakova, D. Mehandjiev, J. Mol. Catal. A 213 (2004) 235–240.
[53] C.H. Kim, L.T. Thompson, J. Catal. 230 (2005) 66–74.
[54] G.M. Veith, A.R. Lupini, S. Rashkeev, S.J. Pennycook, D.R. Mullins, V. Schwartz, C.A. Bridges, N.J. Dudney, J. Catal. 262 (2009) 92–101.
[55] R. Zanella, S. Giorgio, C.H. Shin, C.R. Henry, C. Louis, J. Catal. 222 (2004) 357–367.
[56] T. Tsuchida, J. Kuboa, T. Yoshioka, S.J. Sakuma, T. Takeguchi, W. Ueda, J. Catal. 259 (2008) 183–189.
[57] R. Zanella, L. Delannoy, C. Louis, Appl. Catal. A 291 (2005) 62–72.